Nanoscale

Cite this: *Nanoscale*, 2012, **4**, 3990

www.rsc.org/nanoscale

PAPER

Structural and electronic properties of bilayer and trilayer graphdiyne†

Qiye Zheng,[a] Guangfu Luo,[ac] Qihang Liu,[a] Ruge Quhe,[ab] Jiaxin Zheng,[ab] Kechao Tang,[a] Zhengxiang Gao,[a] Shigeru Nagase[c] and Jing Lu*[a]

Received 13th March 2012, Accepted 3rd May 2012
DOI: 10.1039/c2nr12026g

Stimulated by the recent experimental synthesis of a new layered carbon allotrope–graphdiyne film, we provide the first systematic *ab initio* investigation of the structural and electronic properties of bilayer and trilayer graphdiyne and explore the possibility of tuning the energy gap *via* a homogeneous perpendicular electric field. Our results show that the most stable bilayer and trilayer graphdiyne both have their hexagonal carbon rings stacked in a Bernal way (AB and ABA style configuration, respectively). Bilayer graphdiyne with the most and the second most stable stacking arrangements have direct bandgaps of 0.35 eV and 0.14 eV, respectively; trilayer graphdiyne with stable stacking styles have bandgaps of 0.18–0.33 eV. The bandgaps of the semiconducting bilayer and trilayer graphdiyne generally decrease with increasing external vertical electric field, irrespective of the stacking style. Therefore, the possibility of tuning the electronic structure and optical absorption of bilayer and trilayer graphdiyne with an external electric field is suggested.

Due to the unique ability of carbon to form a wide range of structures, tremendous effort has been devoted to the discovery and study of novel carbon allotropes during the past 20 years. Numerous new important members such as zero-dimensional fullerene,[1] quasi-one-dimensional carbon nanotube[2] and two-dimensional graphene[3] have been synthesized and added to the carbon family. It is believed that highly conjugated, carbon-rich organic molecules with its tunable structural and opto-electronic properties can perform as promising candidates for applications in the next-generation electronic and optoelectronic devices.[4–7] Recently, a new carbon allotrope–graphdiyne has been fabricated as low dimensional nanostructures in forms of large-area-multilayer film,[8,9] nanotubes,[10] and nanowires.[11] The geometrical structure of monolayer graphdiyne is demonstrated in Fig. 1(a). Since it contains two sp hybridized acetylenic linkages between neighboring benzoic rings, graphdiyne was predicted to be one of the "most stable diacetylenic carbon allotropes" with extreme hardness, high thermal resistance and conductivity and synthetic approachability.[9] Density functional theory (DFT) calculations predicted that monolayer graphdiyne is a semiconductor with a direct bandgap of 0.44,[25] 0.46,[12] or 0.53 eV[13] at the Γ point. Remarkably, the calculated electron mobility of monolayer graphdiyne is up to 10^5 cm^2 V^{-1} s^{-1} at room temperature,[12] which is close to the value of graphene,[14] while the measured mobility of synthesized graphdiyne nanowires is 7.1×10^2 cm^2 V^{-1} s^{-1} at room temperature.[11] In addition, the experimental conductivity of multilayer graphdiyne films and graphdiyne nanowires is 2.516×10^{-4} and 1.9×10^3 S m^{-1}, respectively, typical of a semiconductor.[11] Therefore, the future potential application of graphdiyne in the realm of nanoelectronics and photoelectronics is highly anticipated.

With the progress in the study of the monolayer graphdiyne, it is natural and necessary to turn our attention to the few-layer systems of this carbon allotrope, especially the bilayer and trilayer ones. Various stacking manners exist when two and three monolayer graphdiyne are stacked together, and the electronic structures of bilayer and trilayer graphdiyne may depend on the stacking manner. Thus, the most stable stacking manner of bilayer and trilayer graphdiyne should be clarified. Since it is well known that the bandgap of few-layer systems, like bilayer graphene, can be tuned by applying a vertical external electric field,[15] it is interesting to explore the tuning of the electronic structure of bilayer and trilayer graphdiyne with a similar method. In this work, we first investigate the stability of different stacking manners and their relevant electronic structures (mainly about effective mass, and electron mobility), and then the possible bandgap engineering *via* perpendicular electric field in bilayer graphdiyne by using a DFT method. Finally these studies are extended to trilayer graphdiyne.

[a]*State Key Laboratory of Mesoscopic Physics and Department of Physics, Peking University, Beijing 100871, P. R. China. E-mail: jinglu@pku.edu.cn*
[b]*Academy for Advanced Interdisciplinary Studies, Peking University, Beijing 100871, P. R. China*
[c]*Department of Theoretical and Computational Molecular Science, Institute for Molecular Science, Okazaki, 444-8585, Japan*

† Electronic supplementary information (ESI) available: Calculated band structures under three different electric field strengths of bilayer graphdiyne with the acetylenic bond of the top layer stacked over the benzoic ring of the bottom layer; comparison of the electronic structure of bilayer graphdiyne stacked in the AB(β1) manner calculated with and without vdW correction. See DOI: 10.1039/c2nr12026g

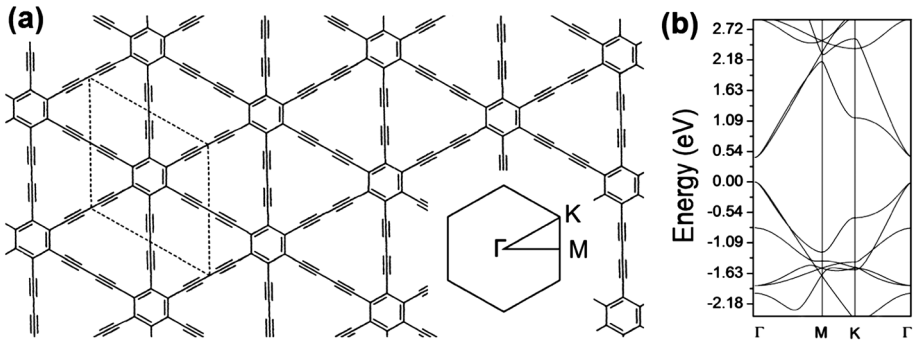

Fig. 1 (a) Geometrical structure of single graphdiyne sheet where the unit cell is drawn with a dashed line. The lower right corner shows the in-plane Brillouin zone of graphdiyne with high-symmetry points labeled. It also represents the projection of both the AA and the AAA stacking arrangement structures of bilayer and trilayer graphdiyne onto the lattice plane. (b) Band structure of monolayer graphdiyne given by DFT–GGA calculation with dispersion correction.

In this article, all DFT calculations are performed based on the PW91 form of generalized gradient approximation (GGA) for exchange-correlation functional from Perdew and Wang[16] with the inclusion of dispersion correction proposed by Ortmann, Bechstedt, and Schmidt.[17] Considering the significant role of long-range interlayer interaction in determining the graphdiyne structure and binding energy, this corrected DFT method is expected to give more reliable results than pure DFT method since it provides a dramatic improvement over pure DFT or pure forcefield methods in terms of the structure description and energies for molecular crystals.[18] Geometry optimization is performed by using all-electron triple numerical basis set plus polarization (TNP) implemented in the DMol^3 package[19,20] with a force tolerance of 0.001 eV Å^{-1} per atom. A 12 × 12 × 1 Monkhorst–Pack[21] k-point mesh is applied to sample the Brillouin zone. Our test shows that the optimized lattice constant and interlayer distance of graphite by this corrected DFT method is 2.457 and 3.340 Å, respectively, which are in good agreement with the experimental values of 2.46 and 3.33 Å, respectively.[22]

The graphdiyne models are simulated within a supercell where the nearby out-of-plane distance between neighbor supercells is set to be larger than 40 Å to avoid the discontinuity of the applied potential and the spurious interactions. The electric field in calculation is characterized as a sawtooth potential along the z direction with its strength ranging from 0 to 1.03 V Å^{-1}. Such a homogeneous field in the region of the graphdiyne layers will be referred to as $E_\perp$. The optimized lattice constant of monolayer graphdiyne is $a = b = 9.45$ Å, in agreement with the previous theoretical values of 9.38,[23] 9.44,[24] 9.48,[12] and 9.46 Å.[25] This lattice parameter is fixed in all the calculations considering that the relatively weak van der Waals (vdW) interaction does not influence this value much (the validity is confirmed by our full geometrical optimization tests for the stable configurations of bilayer graphdiyne) though it is significant to decide the interlayer distance.

To find the stable configurations of bilayer graphdiyne under zero field, we first investigate the optimal relative in-plane position by shifting the upper layer in the primitive cell with a fixed layer distance, and then we relax and optimize the layer distance with the optimized relative in-plane position. Fig. 2(a) demonstrates the total energy of bilayer graphdiyne as a function of the relative in-plane position with a fixed interlayer distance of 3.40 Å (other values of 3.10, 3.30, and 3.50 Å give similar surfaces). In this figure, the origin corresponds to

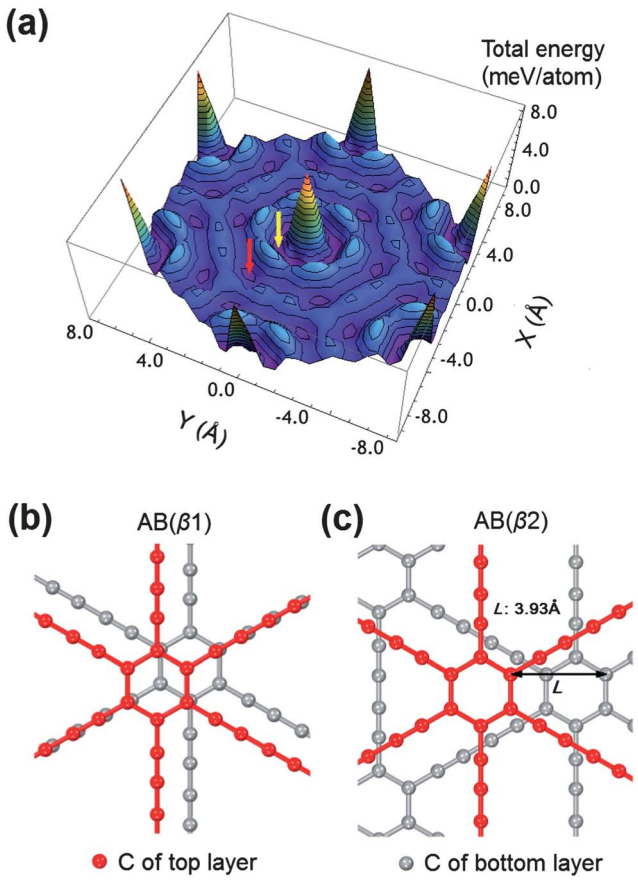

Fig. 2 (a) Energy surface as a function of relative in-plane position specified according to a rainbow-color contour mapping. It is plotted with 81 different relative positions of the two layers in ¼ primitive cell as sampling points, then expanded to the whole area using the lattice symmetry. These sample points are well distributed in the region with the distance of two points set as 0.59 Å. The yellow and red arrows indicate the most and second most stable in-plane position, respectively. Optimized configurations of bilayer graphdiyne named (b) AB(β1) and (c) AB(β2) from top view.

the AA stacking style and has the highest total energy. Two nonequivalent energy minima with close energy are demonstrated by the arrows of different colors, corresponding to two stable stacking arrangements. We refer to the two most stable stacking manners as AB(β1) and AB(β2) (the former is only 0.1 meV per atom more stable than the latter) and show their structures in Fig. 2(b) and (c), respectively. As far as the relative position of the hexagonal carbon ring in the two carbon layers is concerned, the AB(β1) configuration resembles that of the AB stacked graphene while in the AB(β2) configuration the hexagonal ring of the top layer moves along the direction that is perpendicular to the edge of the lower hexagonal ring by 3.93 Å and is located in the triangle region of the diyne chain. Actually, the AB(β2) configuration resembles the stacking manner of bulk graphyne with the highest stability.[13] As shown in Table 1, with vdW correction included, the relaxed interlayer distances of bilayer graphdiyne with the AB(β1) and AB(β2) configurations are $l = 3.42$ and 3.40 Å, respectively, which are comparable with the calculated interlayer distance of graphyne in its most stable stacking manner (3.20 Å)[26] and the measured interlayer distance (3.33 Å) of graphite.[27] The most unstable AA stacking manner has a significantly larger interlayer distance of 3.65 Å because the repulsion between the electron clouds of different layers is maximized in this configuration. In bulk graphyne, the AA stacked structure also has the largest interlayer distance of 3.51 Å.[13] The interlayer binding energies (the total energy difference between two free monolayers and the optimized bilayer structure, abbreviated to BE) of the AB(β1) and AB(β2) configurations are quite similar with BE = 29.5 and 29.4 meV per atom, respectively. These values are about 17% larger than that of the AA one (see Table 1).

As demonstrated in Fig. 3(a)–(c), the electronic structure of bilayer graphdiyne is highly sensitive to the stacking mode. The AB(β1) configuration is semiconducting under zero electric field, with a direct bandgap of 0.35 eV located on the M–Γ path (Fig. 3(a)), which is slightly larger than the largest energy gap (0.25 eV) of bilayer graphene opened by the electric field.[15,28] The AB(β2) configuration is also semiconducting but with a smaller direct bandgap of 0.14 eV at the Γ point (Fig. 3(b)). The most unstable AA stacked structure turns out to be metallic (see Fig. 3(c)) and the underlying mechanism will be discussed later. For comparison, the energy band of optimized monolayer graphdiyne is shown in Fig. 1(b). The resulting bandgap of monolayer graphdiyne (0.46 eV) is in agreement with those reported in previous works using the DFT method (0.44,[25] 0.46,[12] or 0.53[13] and 0.52 eV[25]) and larger than those of bilayer graphdiyne. We calculated the energy bands of bilayer graphdiyne with a certain structure stacked in the AB(β1) manner with and without vdW correction in the ESI† to examine its influence and the difference turns out to be totally negligible. The reason lies in that the vdW correction that we exploit introduces an additional dispersion energy term of the form $f(R)C_6R^{-6}$ in the total energy,[17,29,30] where R is the distance between two atoms and $f(R)$ is the empirical damping function in the total energy which influence the determination of stable structures. However, for a given optimized structure, since the material-specific dispersion coefficient C_6 and $f(R)$ are derived from a fixed set of universal parameters and a fixed damping procedure[31,32] based on previous experimental and theoretical work,[30,31,33–35] the total self-consistent electron density used in the DFT–GGA calculation is intact and thus the band structure is intact. We also note that not only the two most stable bilayer graphdiyne have bandgaps comparable with three-dimensional graphyne at stable stacking arrangements (ranging from 0.19 to 0.50 eV[13]) but also the AA stacked graphdiyne resembles the situation of graphyne with the same configuration: the band structures of both are in-plane metallic.[13]

Fig. 3(a) and (b) show the band structures of the two most stable bilayer graphdiyne under $E_\perp = 0.500$ eV Å^{-1}. It is found that their bandgaps are significantly reduced by the external electric field because of the degeneracy lift near the Γ point (the cause will be discussed later). The bandgap variations of these two structures as a function of the vertical electric field ranging from 0–1.03 V Å^{-1} are plotted in Fig. 4 with the smallest induced bandgaps given in Table 1. The bandgap of AB(β1) monotonically decreases from 0.35 to 0.10 eV while that of AB(β2) decreases from 0.14 to 0.08 eV. The nonmonotonic change of AB(β2) bandgap curve at $E_\perp = 0.411$ V Å^{-1} is due to the movement of the bandgap position from the Γ point to the M–Γ path. We also consider a configuration with the acetylenic bond of the top layer stacked over the benzoic ring of the bottom layer. This configuration is a saddle in the potential surface and it is 0.6 meV per atom less stable than the AB(β1) stacked bilayer graphdiyne. The band structures of this configuration in different electric fields are provided in the ESI.† The bandgaps are 0.16, 0.12, and 0.11 eV when the external vertical electric fields are 0, 0.500, and 1.000 V Å^{-1}, respectively. Therefore, we reach a conclusion that regardless of the stacking style, a vertical electrical field generally reduces the bandgap of a semiconducting bilayer graphdiyne.

With the parabolic approximation for the band structure of bilayer graphdiyne near the gap, one can get the effective mass expression $m^* = (h/2\pi)^2[\partial^2\varepsilon(k)/\partial k^2]^{-1}$ at the k point of conductance band minimum (CBM) and valence band maximum (VBM). The effective masses under zero field are $m^*_h = 0.179m_0$ and $m^*_e = 0.162m_0$ in monolayer graphdiyne, which agree well with those calculated in previous work reported by Li *et al.* ($m^*_h = 0.172m_0$ and $m^*_e = 0.162m_0$),[12] $m^*_h = 0.240m_0$ and $m^*_e = 0.148m_0$ in bilayer graphdiyne with AB(β1) configuration, and $m^*_h = 0.095m_0$ and $m^*_e = 0.093m_0$ in the AB(β2) configuration in the Γ–K direction, where m_0 is the electron mass. As

Table 1 Calculated optimal interlayer distance (l), binding energy (BE), bandgap under zero field (Δ_0), and minimum bandgap induced by electric field within the range of 0–1.03 V Å^{-1} (Δ_{min}) of bilayer and trilayer graphdiyne with different stacking styles[a]

	Stacking style	l (Å)	BE (meV/atom)	Δ_0 (eV)	Δ_{min} (eV)
Bilayer	AB(β1)	3.42	29.5	0.35 (*d*)	0.10 (*d*)
	AB(β2)	3.40	29.4	0.14 (*d*)	0.08 (*d*)
	AA	3.65	25.2	0	0
Trilayer	ABA(γ1)	3.40	41.6	0.33 (*i*)	0.05 (*i*)
	ABC(γ2)	3.42	41.4	0.18 (*d*)	0.05 (*d*)
	ABC(γ3)	3.41	41.2	0.32 (*i*)	0.01 (*i*)
	AAA	3.64	33.9	0	0

[a] *d*: direct band gap; *i*: indirect band gap.

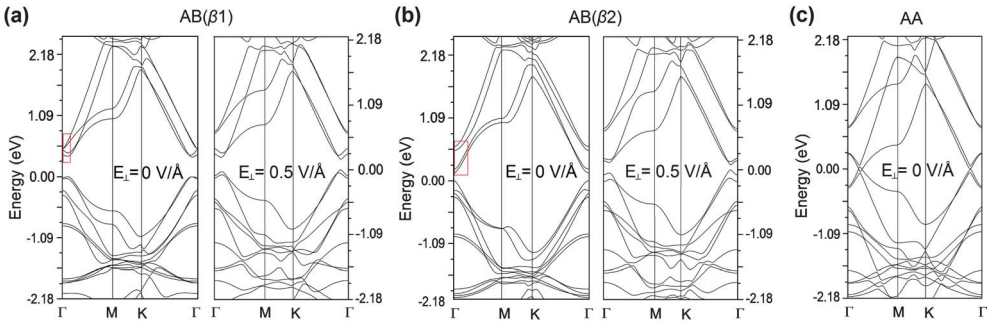

Fig. 3 Band structure of bilayer graphdiyne: (a) AB(β1) configuration at $E_\perp = 0$ (left) and $E_\perp = 0.5$ V Å^{-1} (right), (b) AB(β2) configuration at $E_\perp = 0$ (left) and $E_\perp = 0.5$ V Å^{-1} (right) and (c) AA configuration at zero field. The valence band top of the semiconductor and the Fermi level of the metal are set to zero. The two red boxes in (a) and (b) indicate the two groups of bilayer graphdiyne bands whose energy difference (between the medium energy value of each group at the Γ point) stems from the monolayer LUMO and LUMO+1 interaction.

demonstrated in Fig. 4, with increasing electric field, the effective masses initially increase and form a sharp peak at low field strength, and then decrease significantly. The minimum values of effective mass are found at the field strength which also leads to the minimum bandgaps, with $m^*_h = 0.071m_0$, $m^*_e = 0.060m_0$ for the AB(β1) configuration, and $m^*_h = 0.064m_0$, $m^*_e = 0.060m_0$ for the AB(β2) configuration, which are less than half of the value for monolayer graphdiyne.[12] Based on the effective mass approximation, *i.e.* carrier mobility $\mu = e\tau/m^*$, with scattering relaxation time τ taken from the value in monolayer graphdiyne calculated by Li *et al.* (1.91 ps for hole and 17.49 ps for electron on average), we estimate the carrier mobilities of monolayer graphdiyne to be $\mu_h \approx 1.8 \times 10^4$ cm^2 V^{-1} s^{-1} and $\mu_e \approx 1.9 \times 10^5$ cm^2 V^{-1} s^{-1}. If we assume that τ in bilayer graphdiyne is similar with that in monolayer graphdiyne, the zero-field carrier mobilities of bilayer graphdiyne are estimated to be $\mu_h \approx 1.3 \times 10^4$ cm^2 V^{-1} s^{-1} and $\mu_e \approx 2.1 \times 10^5$ cm^2 V^{-1} s^{-1} for the AB(β1) configuration and $\mu_h \approx 3.5 \times 10^4$ cm^2 V^{-1} s^{-1} and $\mu_e \approx 3.3 \times 10^5$ cm^2 V^{-1} s^{-1} for the AB(β2) configuration. Given an unchanged τ, the carrier mobilities at the electric-field-induced minimum effective mass point are approximately $\mu_h \approx 4.7 \times 10^4$ cm^2 V^{-1} s^{-1} and $\mu_e \sim 5.1 \times 10^5$ cm^2 V^{-1} s^{-1} for the AB(β1) configuration and $\mu_h \sim 5.2 \times 10^4$ cm^2 V^{-1} s^{-1} and $\mu_e \approx 5.1 \times 10^5$ cm^2 V^{-1} s^{-1} for the AB(β2) configuration.

In our work, trilayer graphdiyne is constructed based on the assumption that the Bernal stacking mode of the hexagonal rings is optimal between two adjacent layers. In this sense, three possible stacking styles labeled as ABA(γ1), ABC(γ2), and ABC(γ3) are available and shown in Fig. 5(a)–(c). In the ABA(γ1) configuration, the third and first layer coincide (from top view), in the ABC(γ2) configuration, the hexagonal rings of the three layers are aligned, and in the ABC(γ3) configuration, the hexagonal ring of the third layer shares the same edge with that of the first layer. As shown in Table 1, the relaxed interlayer distances in the ABA(γ1), ABC(γ2), and ABC(γ3) configurations are close with $d = 3.40$, 3.42 and 3.41 Å, respectively, while the AAA stacked structure gives dramatically larger interlayer distance of 3.64 Å, like AA stacked bilayer graphdiyne. The first three configurations have quite close binding energy of BE = 41.6, 41.4 and 41.2 meV per atom for the ABA(γ1), ABC(γ2), and ABC(γ3) configuration, respectively. By contrast, the AAA stacked graphdiyne has a much lower BE of 33.9 meV per atom.

The band structure of trilayer graphdiyne is also stacking-dependent, as shown in Fig. 6(a)–(d). In zero field, the ABA(γ1), ABC(γ2) and ABC(γ3) configurations remain semiconducting. Their main properties are summarized in Table 1 too. It is found that bandgaps under zero field (Δ_0) of the ABA(γ1) and the ABA(γ3) configurations are quite close (0.33 and 0.32 eV, respectively) while that of the ABA(γ1) configuration is almost only half (0.18 eV). Like the situation in bilayer graphdiyne, the most unstable trilayer AAA configuration also shows a metallic band structure. In addition, since the bandgap of trilayer graphdiyne with the ABA(γ1) configuration is smaller than that (0.35 eV) of the bilayer structure with AB(β1) stacking style due to the influence of the added layer, there is a high possibility that the bandgap will further decrease with more layers stacked in such a way.

The bandgaps of the three semiconducting trilayer graphdiyne *versus* the external electric field are shown in Fig. 6(e). In all three structures, the bandgaps initially drop significantly with the increasing field strength as $E_\perp$ is less than 0.308 V Å^{-1} and then change quite slowly. The minimum bandgaps (Δ_{min}) differ for different configurations: Δ_{min} of the ABA(γ1) and ABC(γ2) configurations converges to 0.05 eV despite a difference of 0.15 eV in Δ_0; Δ_{min} of the ABC(γ3) configuration converges to a smaller value of 0.01 eV.

In order to explain the changes of the band structure in different configurations and the effect of the external electric field, we calculate the molecular orbitals in monolayer graphdiyne and investigate the influence of the two factors on them. We demonstrate the electronic structure of monolayer graphdiyne in Fig. 1(b), where both the CBM and VBM are doubly degenerate at the Γ point. Fig. 7(a) and (b) shows the wavefunctions of the two degenerate levels at the bottom of the conduction band and we distinguish them by LUMO and LUMO+1, where LUMO is the abbreviation of the lowest unoccupied molecule orbital while LUMO+1 means the adjacent orbital above it. The principle factor responsible for the change of the bandgaps of different configurations in bilayer and trilayer graphdiyne is the interlayer mixing of π orbitals, which removes the degeneracy near the Γ point. Different overlapping degrees lead to different distortions of the bands and different opening up of the bandgap.

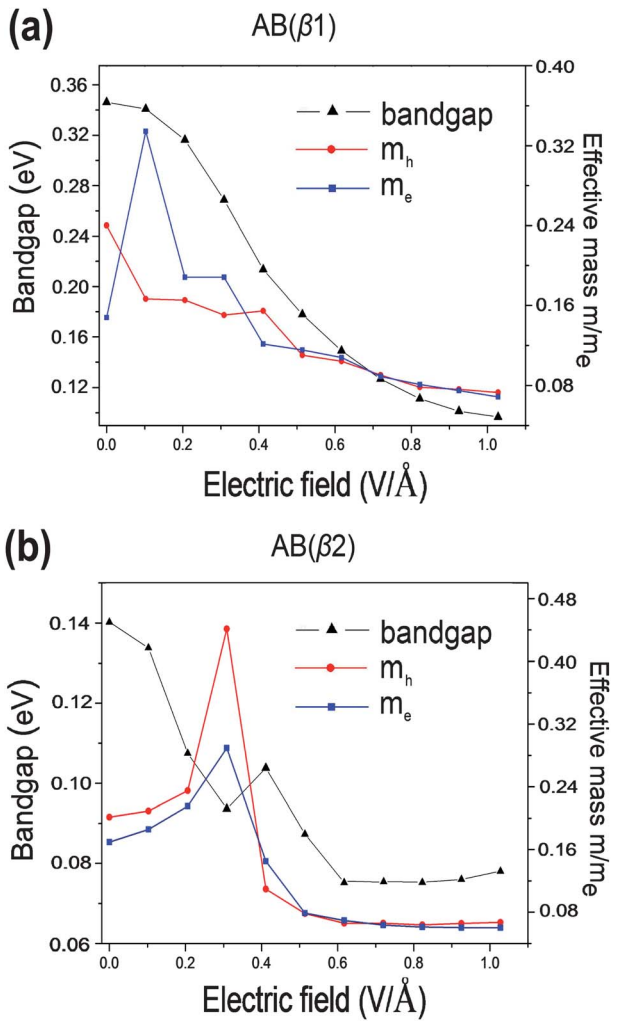

Fig. 4 Bandgap (by the left scale) and effective mass of carriers (m_e and m_h, by the right scale) of AB(β1) (a) and AB(β2) (b) configuration of bilayer graphdiyne as a function of perpendicular electrical field strength. Filled squares and circles indicate the calculated m^*_e and m^*_h. In the AB(β1) configuration, the conductance band minimum (CBM) and valence band maximum (VBM) are located on the M–Γ path while in AB(β2) configuration, they emerge exactly at the Γ point under field strength of 0.411 V Å^{-1} but move to the M–Γ path when field strength surpasses this. The latter fact accounts for the sudden increase of its bandgap shown in the figure.

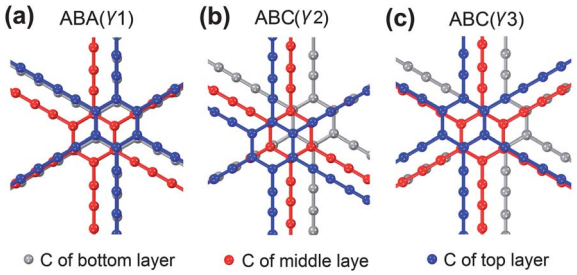

Fig. 5 (a)–(c) Three possible configurations of the trilayer graphdiyne from top view: (a) ABA(γ1), (b) ABC(γ2), and (c) ABC(γ3) configurations. Three different colors are used to distinguish different layers.

When the AA stacked structure is constructed from two monolayer graphdiyne, both the LUMOs between the two layers and the highest occupied orbitals (HOMOs) between the two layers have the largest overlap of either antibonding (*i.e.* the π electron wavefunctions of different layers involved in interaction along their normal direction have different signs), or bonding (wavefunctions have the same sign), styles exclusively compared with other configurations. This leads to the strongest interlayer π–π interactions and thus the largest energy splitting at the Γ point for both the VBM and CBM and consequently causes the metallization of the AA configuration (Fig. 3(c)). As demonstrated in Fig. 7(c) and (d), the LUMO–LUMO+1 overlap of two layers at the Γ point is larger in the AB(β2) configuration than in the AB(β1) configuration. More importantly, in the AB(β1) configuration, half of the overlap is antibonding and half of it is bonding while the AB(β2) configuration constitutes either mostly bonding or mostly antibonding. These two factors cause the coefficient of interaction energy of the Γ point orbitals in the AB(β2) configuration to be larger than that in the AB(β1) configuration in terms of the linear combination of atomic orbitals theory (such as the Hückel molecular orbital method). Therefore, the energy splitting at the Γ point between the LUMO and LUMO+1 groups in the AB(β2) configuration is larger than that in the AB(β1) configuration as demonstrated in Fig. 3(a) and (b) within the red boxes. Such a difference leads to a lower energy of the CBM in the AB(β2) configuration and to a large extent accounts for the smaller bandgap of the AB(β2) configuration compared with that of the AB(β1) configuration.

The tuning of bandgap in bilayer graphdiyne by a vertical electric field can also be understood with the model of molecule orbitals. Fig. 8 schematically demonstrates how the energy gap of bilayer graphdiyne as a result of interaction between relevant monolayer states is reduced by a vertical electric field. In the first place, the splitting of the LUMO as well as HOMO leads to a reduced band gap of bilayer compared with the monolayer. When the bilayer graphdiyne is subject to the perpendicular external field directing from the bottom to top layer ($E_\perp > 0$ in our model), both the HOMO and LUMO of the top layer atoms are raised (see Fig. 8(b)). Thus, the energy difference between the LUMO of the bottom layer and the HOMO of the top layer is reduced with an applied electric field. Besides, the splitting of the monolayer HOMO and LUMO also becomes larger. Consequently, the bandgap of bilayer structure is lowered under an electric field. This model can be expanded to a general semiconducting bilayer. Therefore, it appears that the bandgap of a semiconducting bilayer material can always be reduced *via* a vertical electric field.

The shapes of the energy bands near the Fermi level in trilayer graphdiyne generally resemble those of bilayer graphdiyne but with additional bands (see Fig. 3(a) and (b) and 6(a)–(c)) since the newly added top layer graphdiyne has a symmetrical environment as that of the bottom layer. The mechanism of how their zero-field bandgaps are formed is similar to the situation in the bilayer case as shown in Fig. 8(a). But with more monolayer orbitals involved, the interlayer interactions in the three sampling trilayer systems are stronger (compared with that in bilayer

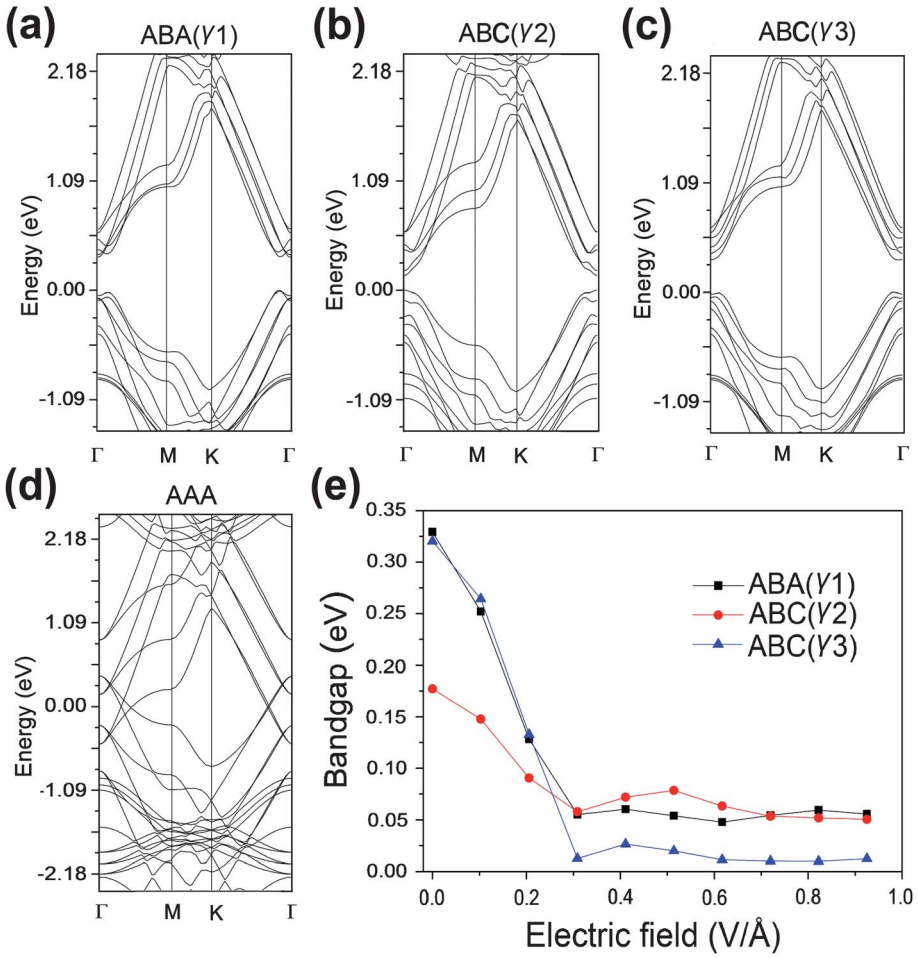

Fig. 6 (a)–(d) Band structure of trilayer graphdiyne configurations of the (a) ABA(γ1), (b) ABC(γ2), (c) ABC(γ3), and (d) AAA configurations under zero field. (e) Bandgap of these three possible trilayer configuration *versus* perpendicular electrical field strength.

AB(β1) configuration), leading to a larger splitting of the HOMO and LUMO at the Γ point. As a result, the Δ_0 values of the three sampling trilayer graphdiyne are smaller than that of bilayer AB(β1) configuration.

In addition, the model of the electric effect in semiconducting bilayer systems can also explain the bandgap reduction of the semiconducting trilayer. However, the energy difference between the LUMO of the bottom layer and the HOMO of the top layer is smaller than that in bilayer because the distance between the top and bottom layers is larger in the trilayer than in the bilayer and the energy shift by a vertical electric field is larger from the $U = E \times l$ relation, where U is static electric potential and E is the homogeneous electric field strength. As a result, the bandgap is generally smaller in a semiconducting trilayer than a bilayer under the same electric field.

It should be noted that the bandgaps of bilayer and trilayer graphdiyne provided by DFT are underestimated to a large extent since the strong electron–electron correlation is not taken into account. The recent calculations demonstrate that the band gap of monolayer graphdiyne is corrected from 0.44 to 1.10 eV upon the inclusion of electron–electron correlation.[36] However, we believe that the dependence of the electronic properties on the stacking manner and tunability of the band gap of bilayer and trilayer graphdiyne with vertical electric field are robust against the inclusion of electron–electron correlation though the band gap is subject to a large enhancement.

In summary, the optimized geometry and electronic band structures of bilayer and trilayer graphdiyne are calculated using DFT–GGA method with dispersion correction. We find that the stacking arrangements showing highest and the second highest stability for bilayer system are the AB(β1) and AB(β2) configuration, respectively, and among several sampling trilayer structures the ABA(γ1) configuration is the most stable one. All of these relatively stable structures are semiconductor: bilayer AB(β1) and AB(β2) configurations possess bandgaps of 0.35 and 0.14 eV, respectively; trilayer ABA(γ1), ABC(γ3), and ABC(γ2) configurations have bandgaps of 0.32, 0.33 and 0.18 eV, respectively. By contrast, the AA and AAA stacked graphdiyne have the lowest stability in their categories and are metallic. Under a vertical electric field, the bandgaps of all the semiconducting configurations generally decrease with increasing field strength. Such properties if supported by further experimental evidence will make few-layer graphdiyne important candidates in the fabrication of tunable nano-scale high performance FET (Field Effect Transistor) and optical devices.

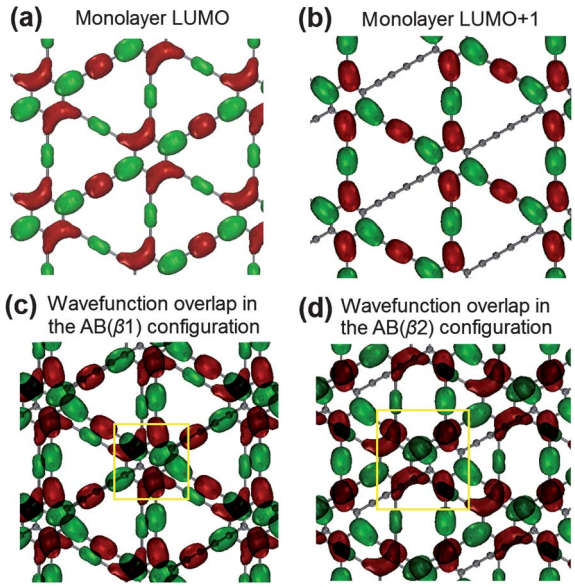

Fig. 7 Wavefunctions of the (a) LUMO, and (b) LUMO+1 in monolayer graphdiyne at the Γ point with red and green isosurfaces denoting different signs of the wave function. Overlap of the LUMO and LUMO+1 electron wavefunctions of the two monolayer graphdiyne with (c) AB(β1) and (d) AB(β2) stacking styles. The two yellow boxes indicate the main overlapped parts (darkened color) within a unit cell.

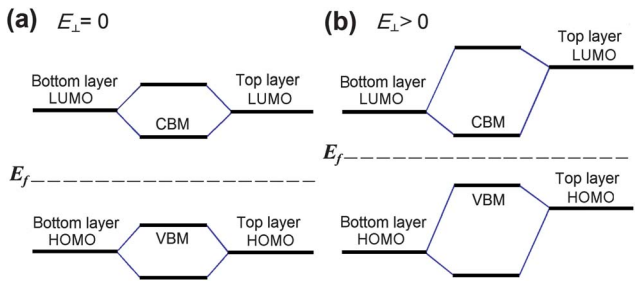

Fig. 8 Schematic energy diagram for bilayer graphdiyne (a) in zero field and (b) a small electric field from bottom to top. The energy levels of monolayers states labeled with "HOMO" and "LUMO" before interaction actually indicate those states at the k points of the bilayer CBM and VBM.

Acknowledgements

This work was supported by the NSFC (grant nos 10774003), National 973 Projects (no. 2007CB936200, MOST of China), Program for New Century Excellent Talents in University of MOE, and National Foundation for Fostering Talents of Basic Science (no. J1030310 / no. J1103205) of China, and Grant-in-Aid for Next Generation Super Computing Project (Nanoscience Program) and Specially Promoted Research from the MEXT in Japan.

References

1 H. W. Kroto, A. W. Allaf and S. P. Balm, *Chem. Rev.*, 1991, **91**, 1213–1235.
2 S. Iijima, *Nature*, 1991, **354**, 56–58.
3 A. K. Geim and K. S. Novoselov, *Nat. Mater.*, 2007, **6**, 183–191.
4 F. Diedericht and M. Kivala, *Pure Appl. Chem.*, 2008, **80**, 411–427.
5 F. Diederich, *Chem. Commun.*, 2001, 219–227.
6 K. Mullen, J. S. Wu and W. Pisula, *Chem. Rev.*, 2007, **107**, 718–747.
7 U. H. F. Bunz, Y. Rubin and Y. Tobe, *Chem. Soc. Rev.*, 1999, **28**, 107–119.
8 H. B. Liu, J. L. Xu, Y. J. Li and Y. L. Li, *Acc. Chem. Res.*, 2010, **43**, 1496–1508.
9 Y. L. Li, G. X. Li, H. B. Liu, Y. B. Guo, Y. J. Li and D. B. Zhu, *Chem. Commun.*, 2010, **46**, 3256–3258.
10 Y. L. Li, G. X. Li, X. M. Qian, H. B. Liu, H. W. Lin, N. Chen and Y. J. Li, *J. Phys. Chem. C*, 2011, **115**, 2611–2615.
11 X. Qian, Z. Ning, Y. Li, H. Liu, C. Ouyang, Q. Chen and Y. Li, *Dalton Trans.*, 2012, **41**, 730–733.
12 Z. G. Shuai, M. Q. Long, L. Tang, D. Wang and Y. L. Li, *ACS Nano*, 2011, **5**, 2593–2600.
13 N. Narita, S. Nagai, S. Suzuki and K. Nakao, *Phys. Rev. B: Condens. Matter*, 2000, **62**, 11146–11151.
14 K. I. Bolotin, K. J. Sikes, J. Hone, H. L. Stormer and P. Kim, *Phys. Rev. Lett.*, 2008, **101**, 096802.
15 F. Wang, Y. B. Zhang, T. T. Tang, C. Girit, Z. Hao, M. C. Martin, A. Zettl, M. F. Crommie and Y. R. Shen, *Nature*, 2009, **459**, 820–823.
16 J. P. Perdew and Y. Wang, *Phys. Rev. B: Condens. Matter*, 1992, **45**, 13244–13249.
17 F. Ortmann, F. Bechstedt and W. G. Schmidt, *Phys. Rev. B: Condens. Matter Mater. Phys.*, 2006, **73**, 205101.
18 A. Asmadi, M. A. Neumann, J. Kendrick, P. Girard, M. A. Perrin and F. J. J. Leusen, *J. Phys. Chem. B*, 2009, **113**, 16303–16313.
19 B. Delley, *J. Chem. Phys.*, 1990, **92**, 508–517.
20 B. Delley, *J. Chem. Phys.*, 2000, **113**, 7756–7764.
21 H. J. Monkhorst and J. D. Pack, *Phys. Rev. B: Solid State*, 1976, **13**, 5188–5192.
22 M. C. Schabel and J. L. Martins, *Phys. Rev. B: Condens. Matter*, 1992, **46**, 7185–7188.
23 S. X. Du, L. D. Pan, L. Z. Zhang, B. Q. Song and H. J. Gao, *Appl. Phys. Lett.*, 2011, **98**, 173102.
24 N. Narita, S. Nagai, S. Suzuki and K. Nakao, *Phys. Rev. B: Condens. Matter*, 1998, **58**, 11009–11014.
25 K. Srinivasu and S. K. Ghosh, *J. Phys. Chem. C*, 2012, **116**, 5951–5956.
26 M. J. Buehler and S. W. Cranford, *Carbon*, 2011, **49**, 4111–4121.
27 Y. Baskin and L. Meyer, *Phys. Rev.*, 1955, **100**, 544–544.
28 E. V. Castro, K. S. Novoselov, S. V. Morozov, N. M. R. Peres, J. M. B. L. Dos Santos, J. Nilsson, F. Guinea, A. K. Geim and A. H. C. Neto, *Phys. Rev. Lett.*, 2007, **99**, 216802–216805.
29 S. Grimme, *J. Comput. Chem.*, 2004, **25**, 1463–1473.
30 L. Zhechkov, T. Heine, S. Patchkovskii, G. Seifert and H. A. Duarte, *J. Chem. Theory Comput.*, 2005, **1**, 841–847.
31 X. Wu, M. C. Vargas, S. Nayak, V. Lotrich and G. Scoles, *J. Chem. Phys.*, 2001, **115**, 8748–8757.
32 Q. Wu and W. T. Yang, *J. Chem. Phys.*, 2002, **116**, 515–524.
33 F. London, *Z. Phys.*, 1930, **63**, 245–279.
34 Y. K. Kang and M. S. Jhon, *Theor. Chim. Acta*, 1982, **61**, 41–48.
35 K. J. Miller, *J. Am. Chem. Soc.*, 1990, **112**, 8533–8542.
36 G. F. Luo, X. M. Qian, H. B. Liu, R. Qin, J. Zhou, L. Z. Li, Z. X. Gao, E. G. Wang, W. N. Mei, J. Lu, Y. L. Li and S. Nagase, *Phys. Rev. B: Condens. Matter Mater. Phys.*, 2011, **84**, 075439.

